



Characterization of dissolved organic matter fluorescence in the South Atlantic Bight with use of PARAFAC model: Relationships between fluorescence and its components, absorption coefficients and organic carbon concentrations

Piotr Kowalczyk^{a,*}, William J. Cooper^b, Michael J. Durako^c, Amanda E. Kahn^c,
Michael Gonsior^b, Heather Young^c

^a Institute of Oceanology, Polish Academy of Sciences, ul. Powstańców Warszawy 55, PL-81-712, Sopot, Poland

^b Urban Water Research Center and Department of Civil and Environmental Engineering University of California, Irvine, CA 92697-2175, United States

^c The University of North Carolina Wilmington, Center for Marine Science, 5600 Marvin Moss Lane, Wilmington, NC 28409, United States

ARTICLE INFO

Article history:

Received 26 February 2009

Received in revised form 27 July 2009

Accepted 19 October 2009

Available online 30 October 2009

Keywords:

Chromophoric dissolved organic matter

Absorption

Fluorescence

Excitation emission

Matrix

PARAFAC model

Dissolved organic carbon

Organic carbon flux

South Atlantic Bight

ABSTRACT

In this study, the CDOM absorption coefficient at 350 nm [$a_{\text{CDOM}}(350)$] and CDOM excitation emission matrix (EEM) fluorescence were used to estimate annual fluxes of dissolved organic carbon (DOC) from the Cape Fear River to Long Bay in the South Atlantic Bight. Water samples were collected during a 3.5 year period, from October 2001 through March 2005, in the vicinity of the Cape Fear River (CFR) outlet and adjacent Onslow Bay (OB). Parallel factor analysis (PARAFAC) of CDOM EEM spectra identified six components: three terrestrial humic-like, one marine humic-like and two protein-like. Empirical relationships were derived from the PARAFAC model between DOC concentration and $a_{\text{CDOM}}(350)$, total fluorescence intensity and the intensities of respective EEM components. DOC concentration and CDOM optical parameters were very well correlated and R^2 values ranged from 0.77 to 0.90. Regression analyses revealed that the non-absorbing DOC fraction, in DOC concentration estimated from CDOM optical parameters, varied with the qualitative composition of the CDOM. DOC concentration and intensity of the humic-like CDOM components characterized by excitation maxima at longer wavelengths have significantly higher estimated non-absorbing DOC compared to the analogous relationships between DOC and intensity of the humic-like CDOM components characterized by excitation maxima at shorter wavelengths. The relationships between DOC concentration and intensity of one of the protein-like components resulted in significantly reduced non-absorbing DOC fraction in DOC concentration estimation. Results of regression analyses between fluorescence intensities of specific EEM components and CDOM-specific absorption coefficients suggest that the relative proportion of humic-like CDOM components (characterized by excitation maximum at longer wavelengths) and the main protein-like component have the most impact on the values of $a_{\text{CDOM}}^*(350)$. Based on the relationships between $a_{\text{CDOM}}(350)$, Cape Fear River flow, and DOC concentrations, DOC fluxes were estimated for 2002, 2003 and 2004. DOC fluxes varied from 1.5 to 6.2×10^{10} g C yr⁻¹, depending on river flow.

© 2009 Elsevier B.V. All rights reserved.

1. Introduction

Oceans play a major role in controlling the world's climate through regulation of atmospheric CO₂ levels by ocean–atmosphere exchange processes (source and sink of CO₂). A large reservoir of carbon is stored mainly in the form of dissolved organic matter (DOM). For this reason, systematic studies of the distribution and cycling of carbon have been conducted since 1980 mainly in the framework of the Joint Global Ocean Flux Studies (JGOFS) program. JGOFS primarily

addressed the central oligotrophic gyres of the Atlantic and Pacific Oceans, and both marine Arctic and Antarctic polar regions. Dissolved organic matter is by far the largest pool of organic matter in the sea. About 97% of all organic carbon in the ocean is bound in DOM (Hansell and Carlson, 1998). The estimated carbon mass of DOC is 685 Gt (Hansell and Carlson, 2001). The mass of DOC in the sea is comparable to the mass of carbon in the Earth's atmosphere as CO₂ and the amount of carbon in terrestrial ecosystems. An understanding of the mechanisms and processes regulating the amount of DOM in the sea is critical in order to understand the global carbon cycle. Therefore, research on marine DOM has intensified over last 30 years (Hedges, 2002). The main result of JGOFS was elucidation of the spatial and temporal variability of DOC in oceanic systems and its sources and

* Corresponding author. Tel.: +48 58 731 1817; fax: +48 58 551 2130.
E-mail address: piotr@iopan.gda.pl (P. Kowalczyk).

sinks on various temporal scales. The dominant source of organic matter in the world's oceans is autochthonous production, which accounts for more than 95% of total organic matter. The input of terrestrial DOM represents only 2–3% of the total oceanic DOM pool, although it may be a dominant source of DOM in coastal zones (Opsahl and Benner, 1997). In the past, DOM has been regarded as a large inert reservoir of carbon in the ocean, which below the oceans' mixed layer is excluded from the current carbon cycle. Numerous studies have revealed that DOM is an active and dynamic component in carbon biogeochemical cycles and plays important roles in marine ecosystems (e.g., Mopper et al., 1991; Hansell and Carlson, 2002; Gonsior et al., 2009). Previous DOC studies were accomplished mainly through field studies and collection of water samples for laboratory analysis (Hansell and Carlson, 2001, 2002). To better assess DOC dynamics in various areas of the world oceans, there is a critical need to apply new techniques for DOC observations, including satellite imagery, that offer greater spatial and temporal resolution.

The components of DOM that absorb light, mainly humic substances, cause water to appear yellowish. For that reason, this colored fraction of DOM was previously named 'Gelbstoff', or yellow substances (Kalle, 1966), but is now commonly referred to as CDOM (chromophoric dissolved organic matter). CDOM absorption is highest in the UV wavelengths and decreases exponentially with increased wavelength (Jerlov, 1976; Kirk, 1994). CDOM is one of the major determinants of the optical properties of natural waters and it directly affects both the quantity and spectral quality of light in the water column (Jerlov, 1976; Blough and Del Vecchio, 2002; Hargreaves, 2003). Through its effects on solar radiation in the water column, CDOM may stimulate or hinder primary production and temperature stratification (e.g., Mopper and Kieber, 2002). Photochemical reactions of CDOM produce inorganic carbon, low-molecular-weight organic compounds, trace gases, and phosphorus- and nitrogen-rich compounds (e.g., Vähätalo and Zepp, 2005; Stedmon et al., 2007). CDOM can produce complexes with trace metals that are later released into the marine environment during DOM remineralization. Therefore, the ability to differentiate and quantify sources of CDOM and the factors underlying its variability is fundamentally important for understanding biogeochemical cycles in the oceans.

Although the principle optical property of CDOM was established almost 50 years ago, optical properties of CDOM were not a major focus of investigations, even with the JGOFS programs. Ocean color remote sensing has been the primary driver for optical studies of CDOM in the oceans for the last two decades. There are two main aspects responsible for the increased interest in CDOM and its characterization for remote sensing. First, the absorption spectra of chlorophyll *a* and CDOM overlap in the blue region of the electromagnetic spectrum. Application of early remote sensing algorithms, which had not taken into account the presence of CDOM, led to a significant overestimation of chlorophyll *a* concentration, especially in coastal oceans and semi-enclosed seas (IOCCG, 2000). Second, the optical properties of CDOM have allowed ocean color remote sensing studies of organic carbon cycling on global and regional scales. Technological developments in observational techniques, both remote and *in situ*, applied in studies of global biogeochemical cycles, resulted in a better understanding of CDOM distribution in the ocean due to increased sampling resolution in time and space and by linking CDOM with other environmental parameters that control its variability. The number of publications on optical properties of CDOM, its distribution and spatial and temporal variability, and on modification of CDOM optical properties by natural processes has grown considerably during the last two decades. Critical overviews of results have been presented for the numerous studies in coastal environments (Blough and Del Vecchio, 2002, and references therein) and in open oceanic waters (Nelson and Siegel, 2002, and references therein).

Del Castillo (2005) assessed the influence of CDOM on apparent optical properties of sea water and its impact on development of

empirical ocean color retrieval algorithms to separate remote sensing reflectance spectra by the contributions of optically active constituents of sea water. In the latest review on CDOM optical properties, Coble (2007) assessed a novel approach to studies on CDOM fluorescence properties and methods leading to a better understanding of cycling of identified CDOM components in aquatic environments. A number of physical, chemical and biological processes all influence the distribution and optical properties of CDOM (see cited reviews and reference therein for detailed descriptions). Among the most important are export of terrestrially-derived CDOM to oceans and its dilution in oceanic waters, photochemical bleaching, bacterial degradation and autochthonous production of CDOM by plankton.

In situ and remote sensing measurements of optical properties of CDOM are easy to conduct and make the use of CDOM absorption or fluorescence as a proxy for DOC concentration very attractive. Although CDOM contributes approximately 20% to the total DOC pool in the open ocean and up to 70% in coastal areas (Coble, 2007), a direct link establishing a global relationship between CDOM and DOC has not been attained. CDOM is a complex mixture of heterogeneous organic compounds, each having individual optical properties. Therefore, the estimation of the universal bulk carbon-specific CDOM absorption coefficient, $a^*_{\text{CDOM}}(\lambda)$, defined as the ratio $a_{\text{CDOM}}(\lambda)/\text{DOC}$, seems almost unfeasible (Woźniak and Dera, 2007). Another aspect that complicates a global DOC–CDOM relationship, is that processes responsible for production, decomposition and distribution of the bulk DOC and CDOM components are decoupled in oceanic systems.

In oligotrophic subtropical gyres and central open ocean areas not in close proximity to terrestrial influence, there is a significant time phase shift between maximum DOC concentration produced by phytoplankton blooms and maximum CDOM absorption (Nelson et al., 1998; Siegel et al., 2002). Additionally, in surface waters, CDOM absorption is quickly diminished by intensive photobleaching (Vodacek et al., 1997; Johannessen et al., 2003). Below the mixing zone, there is usually an increase in CDOM absorption in contrast to the decrease in DOC levels (Nelson et al., 2007). The strong correlation between both $a_{\text{CDOM}}(\lambda)$ and DOC exists only in areas where variability of both parameters is controlled by mixing of fresh and oceanic waters. Several studies have reported a good correlation between $a_{\text{CDOM}}(\lambda)$ and DOC in coastal areas (Green and Blough, 1994; Vodacek et al., 1995; Ferrari et al., 1996; Vodacek et al., 1997; Ferrari, 2000; Chen et al., 2002; Rochelle-Newall and Fisher, 2002; Del Vecchio and Blough, 2004). These local and highly-variable relationships are valuable for studying carbon cycling in coastal areas because they enable the application of ocean color remote sensing to capture synoptic DOC distribution in fine spatial and temporal resolution (e.g., Del Castillo and Miller, 2008).

We have collected an extensive time series of CDOM optical property data between 2001 and 2005 in the South Atlantic Bight. In this study, fluorescence excitation emission matrix (EEM) spectra were reassessed using a novel technique of statistical modeling, parallel factor analysis, PARAFAC. PARAFAC modeling was applied to identify purely statistical fluorophore components that are responsible for specific regions within EEM spectra (Stedmon et al., 2003). This new approach resulted in the identification of six components (three terrestrial humic-like, one marine humic-like and two protein-like) and established compositional characteristics of CDOM in contrasting waters in the study area as well as revealing temporal variability of derived components (Kowalczyk et al., 2009). Results from PARAFAC modeling and data sets of $a_{\text{CDOM}}(350)$ and DOC concentrations were used to achieve the following: i) establish relationships between CDOM fluorescence intensity, absorption coefficient and DOC concentration; ii) assess variability of the carbon-specific CDOM absorption coefficient, $a^*_{\text{CDOM}}(350)$ along a salinity gradient; iii) assess the impact of different CDOM components identified by PARAFAC on $a^*_{\text{CDOM}}(350)$ and carbon-specific CDOM fluorescence; and iv) apply the derived relationships to estimate DOC export by the Cape Fear River to the coastal ocean under different hydrological regimes.

2. Materials and methods

2.1. The study area

The South Atlantic Bight (SAB), defined as the shoreline and the continental shelf from Cape Hatteras to Cape Canaveral, is largely a coastal plain that grades gently into a wide (50–100 km) shelf. The shelf extends to the east until it meets the Gulf Stream. Much of the shoreline consists of barrier islands separated by shifting inlets and riverine estuaries, sounds, lagoons, salt marshes and the Intracoastal Waterway. River input is sporadic. Some areas, like southern Onslow Bay (OB), are sediment-starved with little river input, whereas just south of this area is the Cape Fear River (CFR), North Carolina's largest and most industrialized river system. The CFR watershed is one of the major river systems in the southeastern USA, draining most of the Piedmont coastal plain into the coastal ocean off North and South Carolina and acting as a point source of inorganic and organic nutrients and anthropogenic pollutants into the coastal ocean (Mallin et al., 2000). The entire region is subject to frequent flooding, numerous extreme storm events and chronic erosion problems. Summaries of previous studies of physical, chemical and biological properties of the continental shelf of the SAB are given by Atkinson et al. (1985).

Due to the social and economical importance of the Carolinas' coastal region, environmental monitoring is increasingly important within the SAB. The University of North Carolina Wilmington began an inter-disciplinary, long-term Coastal Ocean Research and Monitoring Program (CORMP) to understand the physical, biological, chemical and geological aspects of this southern region, as well as impacts of natural and anthropogenic changes on the coastal-ocean resources and their management. One of the objectives within CORMP was the characterization of optical properties of the waters of Onslow Bay (OB), the Cape Fear River plume and coastal southeastern North Carolina. Changes in the optical properties of water masses may be used to compare physico-chemical processes within, and exchange between, the coastal system of OB and the adjacent estuarine system of the CFR plume. Optical measurements in the CFR plume area and OB were conducted between October 2001 and March 2005. The evolution of the CORMP optical field sampling program and results of optical measurements, have been presented in series of reports (Kowalczyk et al., 2003, 2006a, 2009). Coastal and estuarine waters in this region differ greatly in their inherent and apparent optical properties. End-members of the CFR study region are extremely rich in CDOM. Kowalczyk et al. (2003) showed that within a small geographical area in the CFR plume and adjacent OB, which is under the influence of Gulf Stream waters, the variability in $a_{\text{CDOM}}(350)$ is as great as observed in natural waters world-wide. CDOM concentration and composition are mostly regulated by the amount of precipitation in the CFR watershed, its flow and the conservative mixing of fresh and oceanic waters (Kowalczyk et al., 2009). However, some CDOM regions within the EEM spectra do not follow a conservative mixing pattern. Absorption of CDOM is also one of the most important water constituents influencing variability, magnitude and spectral shape of apparent optical properties (Kowalczyk et al., 2006a) in the CFR plume area.

This report describes a study period from October 2003 to March 2005, when field observations were conducted only in the Cape Fear River plume area. River-plume samples were collected from a sample grid developed for CORMP (see Fig. 1). This grid consists of 7 stations (labeled CFP1 through CFP9) located at the CFR mouth and adjacent inner continental shelf. The grid was designed to study the spatial and temporal extent of the CFR plume. The CFR plume area was sampled monthly (depending on weather) at ebb tide for maximum extent of the plume.

During field observations, the hydrological conditions in the CFR watershed changed dramatically, influencing discharge of CDOM and its optical properties. River discharge data were recorded by USGS at

the last monitoring station before the estuary at Lock 1, Kelly, North Carolina. The spring and summer of 2002 was a period of severe drought in the CFR watershed, which significantly limited river discharge into the coastal ocean (27.9 to 137.8 m³ s⁻¹). Precipitation increased in fall 2002, reaching a maximum during summer 2003. As a result, river discharge increased nearly 10 fold, reaching a maximum in April 2003 (2023 m³ s⁻¹). In August and September 2003, high rainfall and the passage of Hurricane Isabel caused increased CFR discharge ranging from approximately 300 to 1100 m³ s⁻¹. From autumn 2003 until the end of the field observations in March 2005 the CFR flow was highly variable and ranged between 46.6 and 906 m³ s⁻¹, and no extreme flow events were recorded.

2.2. The optical properties of CDOM

Surface water samples for the determination of optical properties of CDOM were collected using a pre-rinsed bucket, and stored in HDPE bottles in ice and processed in the laboratory the following day. Prior to sample storage, HDPE bottles were rinsed with a high volume of DI water and then washed several times with the marine sample water from each site. Surface salinity was measured with a YSI handheld CT meter or a Seabird CTD profiler.

Samples for spectroscopic analyses were allowed to warm to room temperature and pre-filtered through ~0.7 μm GF/F filters to remove the large particles and phytoplankton cells, then filtered again through 0.2 μm, acid-washed and Milli-Q rinsed Gelman Supor[®] polysulfone filters. Absorbance scans from 240 to 800 nm (1 nm slit width) were conducted using 10 cm Suprasil cuvettes on a Cary 1E dual-beam spectrophotometer connected to a micro-computer. Pre-filtered (0.2 μm) Milli-Q water was used in the reference cell. Absorbance measurements at each wavelength (λ) were baseline corrected by subtracting the mean absorbance calculated in the spectral range from 650 to 700 nm. The required corrections were generally less than 0.002. CDOM absorption coefficients $a_{\text{CDOM}}(\lambda)$ m⁻¹ at each wavelength (λ) were calculated according to Kirk (1994):

$$a_{\text{CDOM}}(\lambda) = 2.303A(\lambda) / l \quad (1)$$

where $A(\lambda)$ is the corrected spectrophotometer absorbance reading at wavelength λ and l is the optical path length in meters. A conservative detection limit of 0.046 m⁻¹, corresponding to an absorbance of 0.002 with 10 cm cells on the spectrophotometer, was estimated from repeated scans of Milli-Q water processed as a sample. Following the recommendations of recent studies (see: Stedmon et al., 2000; Blough and Del Vecchio, 2002), the spectral slope of the absorption spectrum S was calculated by applying a simple exponential model to fit the offset-corrected absorption spectrum at a spectral range from 300 to 500 nm. This method of spectral slope calculation is less dependent on the spectral range used. The spectral range was reduced (300–450 nm) for samples collected at the shelf break because of the very low absorption at longer wavelengths.

Samples for fluorescence were treated in the same manner as those for absorbance measurements. Highly-absorbing samples were diluted with Milli-Q water to the point where $A(350)$ (1 cm path length) was ≤0.02 to minimize inner-filtering effects (Moran et al., 2000; Zepp et al., 2004). Excitation emission matrix (EEM) fluorescence properties were determined on a Jobin Yvon SPEX FluoroMax-3 scanning fluorometer equipped with a 150 W Xe arc lamp and a R928P detector. EEM spectra were constructed by using excitation wavelengths from 250 to 500 nm (5 nm intervals) and scanning emission wavelengths from 280 to 600 nm (5 nm intervals). The instrument was configured to collect the signal in ratio mode with dark offset using 5 nm band pass on both the excitation and emission monochromators. Scans were corrected for instrument configuration using factory-supplied correction factors, which were determined as described in Method 1 of Coble et al. (1993). Comparison of the integrated Raman spectra of Milli-Q

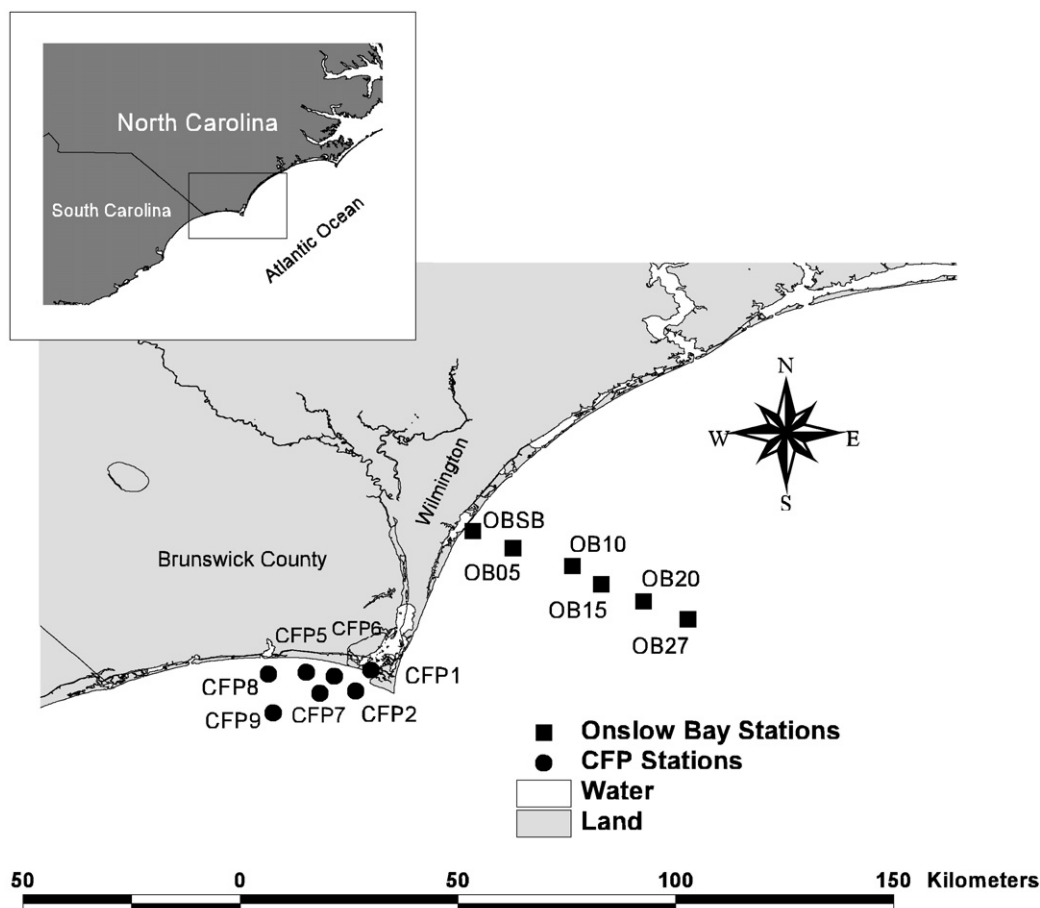


Fig. 1. Location of the sampling stations in the South Atlantic Bight.

water over excitation wavelengths (275ex/303em, 5 nm band pass) measured daily, were used as the test of lamp stability output. Any decrease in lamp efficiency resulted in lamp replacement and instrument calibration. Post-processing of scans was performed using the FL Toolbox 1.91 developed by Wade Sheldon (University of Georgia) for MATLAB® Release 11, (Zepp et al., 2004). This software eliminates Rayleigh and Raman scattering peaks by excising portions (± 10 – 15 nm FW) of each scan centered on the respective scatter peak. The excised data were replaced using three-dimensional interpolation of the remaining data according to the Delaunay triangulation method and constraining the interpolation such that all non-excised data were retained. Following removal of scatter peaks, data were normalized to a daily-determined water Raman intensity (275ex/303em, 5 nm band pass) and converted to Raman-normalized quinine sulfate equivalents (QSE) in ppb (Coble et al., 1998). For samples that required dilution, the scatter-corrected fluorescence of the diluent Milli-Q was subtracted and the resultant fluorescence values were multiplied by the dilution factor to obtain the intensity for the original, undiluted sample. Replicate scans were generally within 5% agreement in terms of intensity and band pass resolution of peak location. The post-processing software did not adequately correct for second-order Raman scattering. The tail of second-order Raman scattering was visible at low signal samples. That error was corrected by subtracting the EEM spectrum of the blank sample of freshly prepared Milli-Q water, measured separately for each data series.

2.3. The PARAFAC modeling

PARAFAC modeling was performed for all measured EEM spectra of CDOM samples collected during the whole field sampling program between October 2001 and March 2005, as described by Kowalczuk

et al. (2009). The EEMs were combined into a three-dimensional data array: 408 samples \times 13 excitations \times 81 emissions, and were modeled by PARAFAC according to the technique described by Bro (1997) and Stedmon et al. (2003). The analysis was carried out in MATLAB with the “Nway toolbox for MATLAB” (Andersson and Bro, 2000). PARAFAC separates the data signal into a set of three linear terms and a residual array.

$$x_{ijk} = \sum_{f=1}^F a_{if} b_{jf} c_{kf} + e_{ijk} \quad i = 1 \dots K \quad j = 1 \dots J \quad k = 1 \dots K. \quad (2)$$

In this application, x_{ijk} is the intensity of fluorescence for the i th sample at emission wavelength j and excitation wavelength k ; a_{if} is directly proportional to the concentration (e.g., mM C) of the f th analyte in the i th sample. b_{jf} is linearly related to the fluorescence quantum efficiency (fraction of absorbed energy emitted as fluorescence) of the f th analyte at emission wavelength j . Likewise, c_{kf} is linearly proportional to the specific absorption coefficient at excitation wavelength k . F defines the number of components in the model, and the residual matrix e_{ijk} represents variability not explained by the model. The model is calculated by minimizing the sum of squared residuals with an alternating least squares algorithm. With this technique, signals from a complex mixture of compounds (in this case, fluorescent DOM) can be separated, with no assumptions on their spectral shape. The number of components is predefined by the operator before the calculating routine starts. The only assumptions in the PARAFAC algorithm are that the components differ from each other spectrally. The PARAFAC model has been run with the non-negativity constraint, as both excitation and emission spectra cannot be negative.

The PARAFAC model returns only relative intensities of derived components (scores), because the specific absorption and quantum yield of fluorescence of components remain unknown. The intensity of the n th component in a given sample, I_n , was calculated as the fluorescence intensity at the peak excitation and emission maximum of the n th component using the following equation:

$$I_n = \text{Score}_n * E_{X_n}(\lambda_{\max}) * E_{M_n}(\lambda_{\max}) \quad (3)$$

where Score_n is the relative intensity of the n th component, $E_{X_n}(\lambda_{\max})$ is the maximum of the excitation loading of the n th component, and $E_{M_n}(\lambda_{\max})$ is the maximum of the emission loading of the n th component derived from the model. The total fluorescence intensity of a given sample was calculated as the sum of the components present in the sample:

$$I_{\text{TOT}} = \sum_1^n I_n \quad (4)$$

2.4. The TOC concentration

Total dissolved organic carbon (DOC) was determined using a Shimadzu TOC-5050A auto analyzer with an ASI 5000 autosampler (Avery et al., 2003) and results are given in $\mu\text{mol/l}$ C. A volume of 75 μL of triplicates of each sample was processed and the concentrations of DOC quantified by the area under the peaks as recorded by the Shimadzu software. All samples were filtered as above prior to TOC analysis.

The carbon-specific CDOM absorption coefficient, $a^*_{\text{CDOM}}(350)$, was calculated as the ratio of the CDOM absorption coefficient $a_{\text{CDOM}}(350)$ and DOC concentration (Eq. (5)). Carbon-specific fluorescence intensity was defined similarly to the carbon-specific CDOM absorption coefficient: the total fluorescence intensity was normalized by the DOC concentration.

$$a^*_{\text{CDOM}}(350) = \frac{a_{\text{CDOM}}(350)}{\text{DOC}} \quad (5)$$

The regression analysis was performed with using the curve fitting tool implemented in Sigma Plot 8.0 data visualization and statistical software. All regression coefficients were tested for significance with the standard Student's t -test. Regression coefficients and determination coefficients, R^2 , given in tables, are statistically significant with confidence levels at least $p < 0.01$.

3. Results

3.1. Spectral characteristics of CDOM components derived from the PARAFAC model

Procedures applied here to derive and evaluate the correctness of the modeled CDOM components were described in detail in Kowalczyk et al. (2009). The PARAFAC model identified three humic-like substances of mainly terrestrial origin, two major ones: component 1 (C1, $\lambda_{\text{ex}}/\lambda_{\text{em}}$ 250/452), and component 2 (C2, $\lambda_{\text{ex}}/\lambda_{\text{em}}$ 250/420), and one secondary humic-like component 4 (C4, $\lambda_{\text{ex}}/\lambda_{\text{em}}$ 270(390)/508). Terrestrially-derived components C1 and C2 commonly occurred in various estuarine, marine and oceanic environments. Component 3 (C3, $\lambda_{\text{ex}}/\lambda_{\text{em}}$ 250(310)/400) has been identified as representing marine humic substances and also as DOM that has been altered by microbial reprocessing (Stedmon and Markager, 2005b). C4 represents fluorophores that have the longest excitation wavelength and broadest excitation band as well as the longest emission wavelength associated with a broad emission band. Such excitation and emission characteristics are associated with terrestrial organic matter composed of high molecular weight and aromatic organic compounds (McKnight et al.,

2001; Stedmon et al., 2003). There were two components that have excitation/emission characteristics similar to fluorescent protein-like compounds and presumably a combination of fluorophores containing the fluorescent amino acids tryptophan and tyrosine bound in proteins. Component 5 (C5, $\lambda_{\text{ex}}/\lambda_{\text{em}}$ 270/332) has excitation/emission characteristics close to tyrosine and component 6 (C6, $\lambda_{\text{ex}}/\lambda_{\text{em}}$ 250(290)/356) has excitation/emission characteristics close to tryptophan. The excitation and emission spectra of individual components identified by the PARAFAC model described by Kowalczyk et al., 2009 are presented in Fig. 2.

3.2. Relationships between $a_{\text{CDOM}}(350)$, total fluorescence intensity and fluorescence intensity of respective CDOM components with DOC concentrations

There was a linear relationship between CDOM absorption coefficient $a_{\text{CDOM}}(350)$ and total fluorescence intensity, I_{TOT} (Fig. 3). The regression coefficient and high determination coefficient suggest that fluorescence may be regarded as a proxy for the absorption coefficient, especially in oceanic waters where CDOM absorption is very low, close to the minimum-detection limit, and the absorption measurement is susceptible to measurement errors. In those waters the fluorescence signal is still quite high ($1.6 \div 5$ QSE). We also analyzed the relationship between $a_{\text{CDOM}}(350)$ and fluorescence intensity of specific components identified by the PARAFAC model (data not shown). Table 1 presents details of the regression analyses. The CDOM absorption coefficient, $a_{\text{CDOM}}(350)$, was best correlated ($R^2 = 0.916$) with fluorescence intensity of the secondary humic-like component (C4), which has excitation/emission characteristics situated at long wavelengths (ex./em. 270(390)/508). The smallest value of the coefficient of determination ($R^2 = 0.712$) was calculated for the relationship between $a_{\text{CDOM}}(350)$ and I_{C5} , the intensity of protein-like fluorophores. The regression between C6 (the second protein-like fluorophores) and the CDOM absorption coefficient was statistically insignificant. Relationships between fluorescence intensities of the remaining components (C1, C2 and C3) and CDOM absorption were also very good (R^2 between 0.828 and 0.902). Both absorption coefficients, $a_{\text{CDOM}}(350)$, and fluorescence intensities were very well correlated with DOC concentration (Fig. 4). According to the regression coefficients (Table 2), non-absorbing DOC estimations were quite similar for DOC vs. $a_{\text{CDOM}}(350)$ ($78.5 \pm 8.5 \mu\text{mol/l}$) and for DOC vs. I_{TOT} ($74.8 \pm 5.6 \mu\text{mol/l}$).

PARAFAC modeling deconvoluted the EEMs into six individual components. The linear relationships between DOC concentration and intensities of respective components are shown on Fig. 5. Values of regression coefficients and coefficients of determinations are given in Table 2. All components except one were well correlated with DOC concentrations. The regression analyses results are statistically significant as indicated by R^2 values ranging between 0.784 and 0.907. Components representing terrestrial humic material (C2, C4) and marine humics (C3) had similar regression coefficients to the linear relationships with DOC concentrations and are among those with highest R^2 values. The principle terrestrial humic material component, C1, was also very well correlated with DOC, but the regression coefficients of this relationship were distinct from the other coefficients listed in Table 2. The main reason for this is the intensity range of C1, which is three times larger than the remaining humic components. C5, one of two components representing protein-like material, was well correlated with DOC concentration in contrast to the regression between intensity of C6 with DOC, which was statistically insignificant. Regression coefficients of the linear relationship for I_{C5} vs. DOC were different from the linear regression coefficients of fluorescence intensity of humic-like components vs. DOC.

Based on linear regression coefficients between intensities of respective components and DOC concentration, the non-absorbing DOC fraction was calculated for DOC concentrations at the 0 value of the

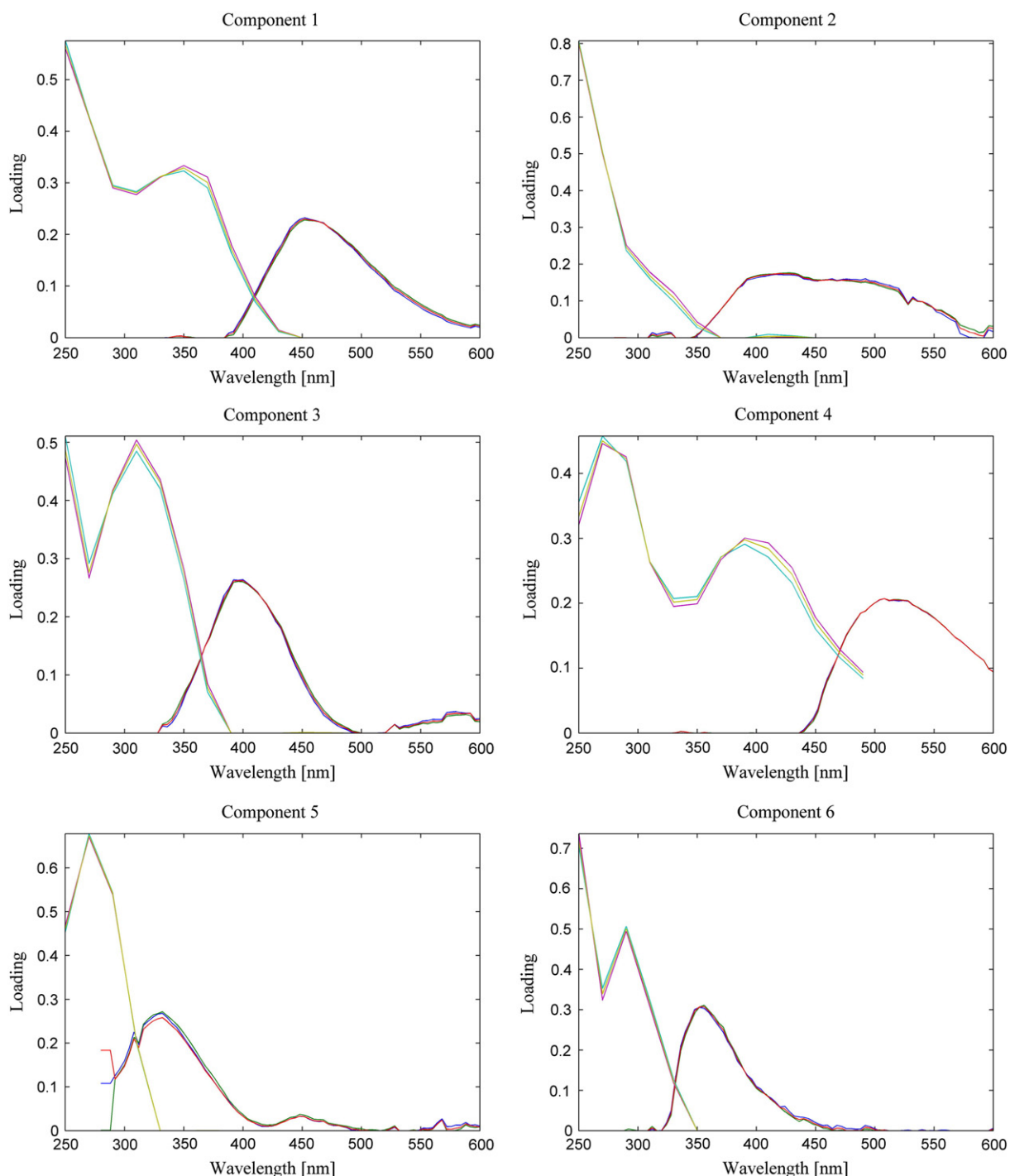


Fig. 2. Excitation and emission spectra of 6 EEM components identified by the PARAFAC model presented in detail in the study by Kowalczyk et al., 2009.

optical signal. Although the regression coefficients were similar for three of five analyzed relationships, the calculated x -intercepts were different. For the non-absorbing DOC fractions, the I_{C1} vs. DOC relationship is $94.0 \pm 6.3 \mu\text{mol/l}$, the I_{C2} vs. DOC relationship is $61.3 \pm 7.1 \mu\text{mol/l}$, the I_{C3} vs. DOC relationship is $77.8 \pm 6.2 \mu\text{mol/l}$, and the I_{C4} vs. DOC relationship is $92.5 \pm 5.6 \mu\text{mol/l}$. The calculated confidence intervals for estimating the non-absorbing DOC fractions for individual components did not overlap, except for C1 and C4, which may suggest that the differences in estimated non-absorbing DOC fractions are statistically significant. The calculated non-absorbing DOC fractions were highest for the components that represent terrestrial humic material, with the longest wavelength of emission maximum, and are associated with

the high molecular weight fraction of DOM. C2 is a secondary humic-like component of terrestrial origin and C3 is associated with marine humic material. Both components have their emission maxima located at shorter wavelengths than C1 and C4, and presumably are much lower in molecular weight. The calculated DOC concentrations of non-absorbing DOC for those two components were significantly lower than the x -intercepts calculated for C1 and C4. The intercept in the linear relationship between I_{C5} vs. DOC was small, compared to other intercepts (Table 2) and positive. Results of Student's t -tests, and standard error of estimation of the intercepts suggest that the intercepts are significantly different from 0 and the regressions should not be forced through the origin. The regression coefficients derived for the linear

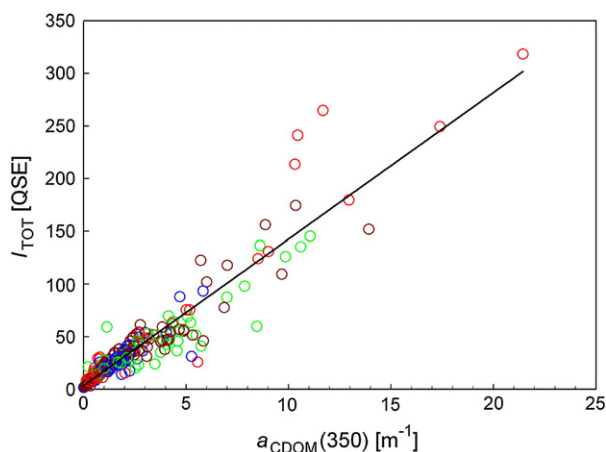


Fig. 3. Relationship between the CDOM absorption coefficient ($a_{\text{CDOM}(350)}$) and total fluorescence intensity (I_{TOT}). Samples collected in different seasons are marked with colors: winter – blue, spring – green, summer – red, autumn – dark red.

relationship between I_{C5} vs. DOC produced a negative x -intercept of the DOC concentration at 0 fluorescence intensity. The concentration cannot be negative; therefore it is assumed that, the uncertainties in both fluorescence and DOC measurements in clear oligotrophic Gulf Stream waters, as well as the inaccuracy of the PARAFAC model, may have produced some numbers of low fluorescence intensity of component C5 and low DOC concentration points, that have impacted the regression calculation. So, the uncertainty in the estimation of the slope of the regression yields an uncertainty in the intercept and estimation of its positive value.

3.3. Relationships between carbon-specific CDOM absorption and fluorescence with $a_{\text{CDOM}(350)}$, total fluorescence intensity and fluorescence intensity of respective CDOM components

Values of the organic carbon-specific CDOM absorption coefficient $a^*_{\text{CDOM}(350)}$ varied within one order of magnitude, between 0.0017 and 0.0360 mM m^{-2} . The highest values of $a^*_{\text{CDOM}(350)}$ were observed in the CFR estuary close to the CFR mouth. The lowest values of $a^*_{\text{CDOM}(350)}$ were observed from sampling stations influenced by oceanic waters. The observed spatial distribution of organic carbon-specific CDOM absorption coefficients in this region was in very good agreement with observations by Del Vecchio and Blough (2004) for the Mid Atlantic Bight. Values of $a^*_{\text{CDOM}(350)}$ were plotted as a function of CDOM absorption coefficient and salinity (Fig. 6, left panels). Similarly, the carbon-specific fluorescence intensities were plotted against the total fluorescence intensity and

Table 1

Results of regression analysis between CDOM absorption coefficient ($a_{\text{CDOM}(350)}$), total fluorescence intensity (I_{TOT}), and intensities of individual components derived from the PARAFAC model.

Parameters	Regression coefficient a	Intercept b	Coefficient of determination R^2	Sample size n
I_{TOT} vs. $a_{\text{CDOM}(350)}$	13.919 ± 0.30	3.455 ± 1.12	0.886	278
I_{C1} vs. $a_{\text{CDOM}(350)}$	6.308 ± 0.13	-1.481 ± 0.48	0.902	278
I_{C2} vs. $a_{\text{CDOM}(350)}$	2.401 ± 0.07	1.431 ± 0.25	0.828	278
I_{C3} vs. $a_{\text{CDOM}(350)}$	2.542 ± 0.06	0.353 ± 0.21	0.879	278
I_{C4} vs. $a_{\text{CDOM}(350)}$	1.820 ± 0.03	-0.365 ± 0.12	0.916	278
I_{C5} vs. $a_{\text{CDOM}(350)}$	0.807 ± 0.03	2.196 ± 0.11	0.712	276
I_{C6} vs. $a_{\text{CDOM}(350)}$	0.156 ± 0.02	1.083 ± 0.09	0.137	278

All variables were fitted to the linear equation $I_n = a^*a_{\text{CDOM}(350)} + b$. Regression coefficients and coefficient of determination are significant at a confidence level $p < 0.01$. Regression coefficients and coefficients of determination that are not statistically significant are marked with italics.

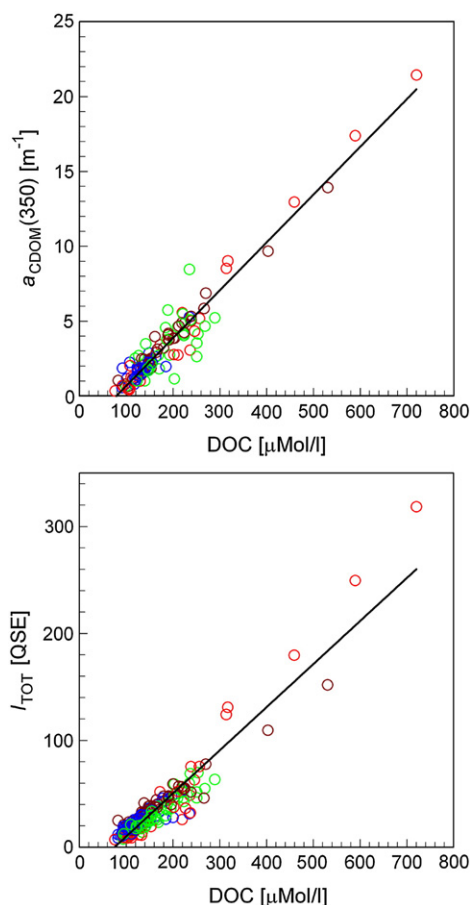


Fig. 4. Relationship between CDOM absorption coefficient ($a_{\text{CDOM}(350)}$) and dissolved organic carbon concentration (upper panel) and relationship between total fluorescence intensity (I_{TOT}) and dissolved organic carbon concentration (lower panel). Samples collected in different seasons are marked with colors: winter – blue, spring – green, summer – red, autumn – dark red.

salinity (Fig. 6, right panels). The distribution of $a^*_{\text{CDOM}(350)}$, as a function of $a_{\text{CDOM}(350)}$, and the distribution of $I_{\text{TOT}}/\text{DOC}$ as a function of total fluorescence intensity were very similar. These distributions were approximated using a hyperbolic function. The approximation was very good as indicated by high values of the coefficient of determination: $R^2 = 0.87$ for $a^*_{\text{CDOM}(350)}$ vs. $a_{\text{CDOM}(350)}$ and $R^2 = 0.80$ for $I_{\text{TOT}}/\text{DOC}$ vs. I_{TOT} . The hyperbolic function distributions suggest an asymptotic relationship between these parameters. This is

Table 2

Results of regression analysis between DOC concentration, CDOM absorption coefficient ($a_{\text{CDOM}(350)}$), total fluorescence intensity (I_{TOT}), and intensities of individual components derived from the PARAFAC model.

Parameters	Regression coefficient a	Intercept b	Coefficient of determination R^2	Sample size n
$a_{\text{CDOM}(350)}$ vs. DOC	0.032 ± 0.001	-2.511 ± 0.18	0.922	115
I_{TOT} vs. DOC	0.403 ± 0.009	-30.134 ± 1.60	0.896	225
I_{C1} vs. DOC	0.190 ± 0.004	-17.853 ± 0.77	0.892	225
I_{C2} vs. DOC	0.066 ± 0.002	-4.046 ± 0.32	0.853	225
I_{C3} vs. DOC	0.072 ± 0.002	-5.598 ± 0.27	0.907	225
I_{C4} vs. DOC	0.057 ± 0.001	-5.275 ± 0.22	0.897	225
I_{C5} vs. DOC	0.020 ± 0.0007	0.702 ± 0.12	0.784	225
I_{C6} vs. DOC	0.003 ± 0.001	1.270 ± 0.20	0.029	225

All variables were fitted to the linear equation $y = a^*\text{DOC} + b$. Regression coefficients and coefficient of determination are significant at a confidence level $p < 0.01$. Regression coefficients and coefficients of determination that are not statistically significant are marked with italics.

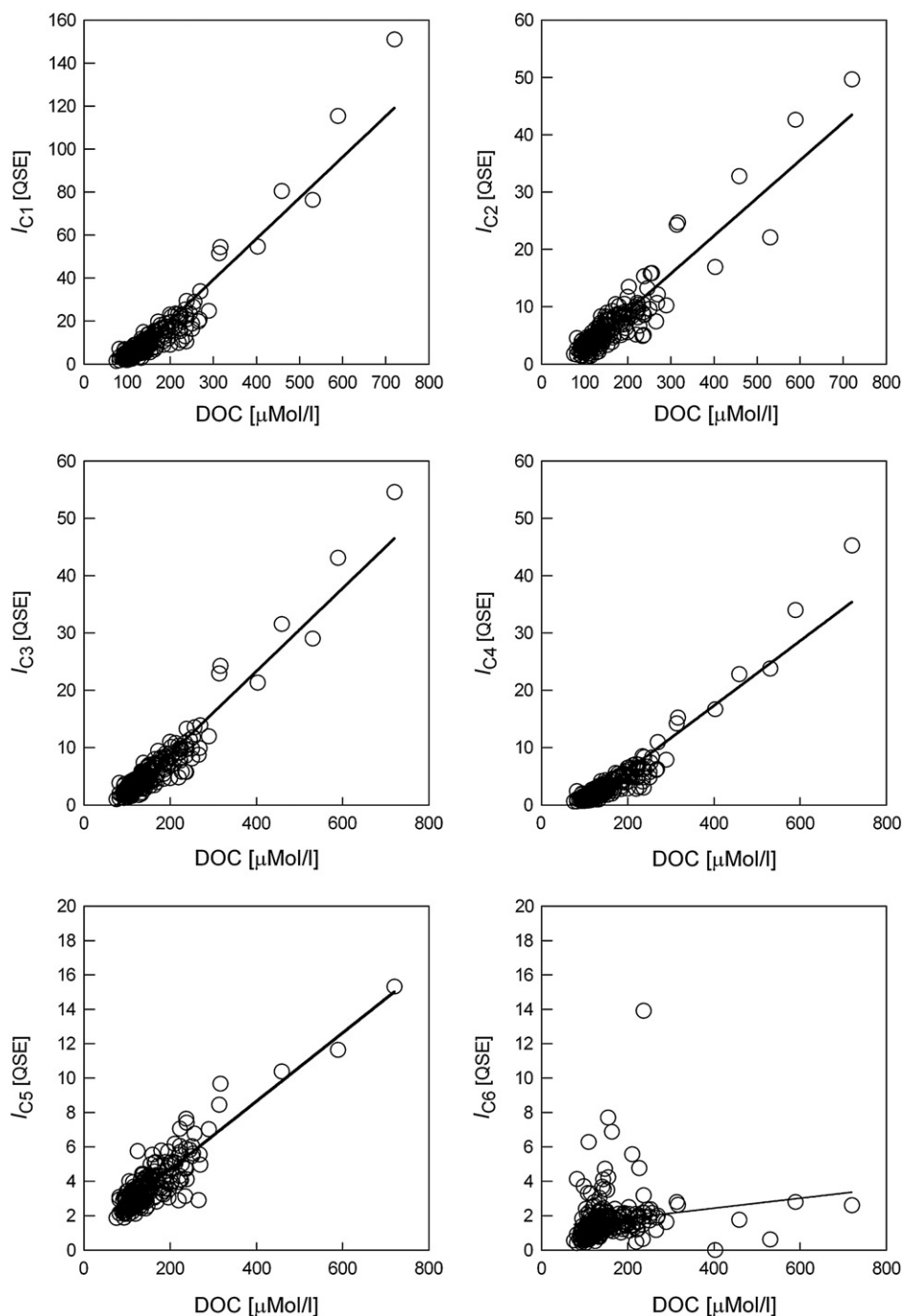


Fig. 5. Relationships between fluorescence intensities of respective components identified by the PARAFAC model (I_n) and dissolved organic carbon concentration.

in good agreement with optical theory, which predicts that absorption cross-section will not increase linearly with an increase of the geometric dimensions and mass of the absorbing molecule/particle. The increase of dimensions and mass of the molecule/particle causes a self-shading effect: the outer structures of the molecule/particle shade the inner structures and effectively decrease the ability to absorb radiant energy. This was clearly visible within our data (Fig. 6 upper panels).

Distributions of the carbon-specific CDOM absorption coefficient and carbon-specific fluorescence intensity as a function of salinity were much more dispersed compared to distributions of both parameters as functions of the optical properties of CDOM. There was a trend towards a decrease of $a^*_{CDOM}(350)$ and I_{TOT}/DOC with increased salinity. At salinities around 30, the slope of the fitted curve

significantly decreased, suggesting that the relationships between $a^*_{CDOM}(350)$ and I_{TOT}/DOC could be approximated using an inverse hyperbolic function. However, there was much scatter in the plots at high salinities (32–36). At those salinities, the influence of the terrestrial source of CDOM lost its dominance on the optical properties of CDOM and non-conservative processes were noticeable (Kowalczyk et al., 2003, 2009). One possible and highly effective process that changes the organic carbon-specific absorption of CDOM is photobleaching (Vodacek et al., 1997). Therefore, the scatter at high salinities may be explained by photochemical processes. Consequently, regression analyses between both optical parameters and salinity could be inaccurate at high salinities, and dilution may not be the only factor influencing the distribution of $a^*_{CDOM}(350)$ and I_{TOT}/DOC values in the salinity gradient.

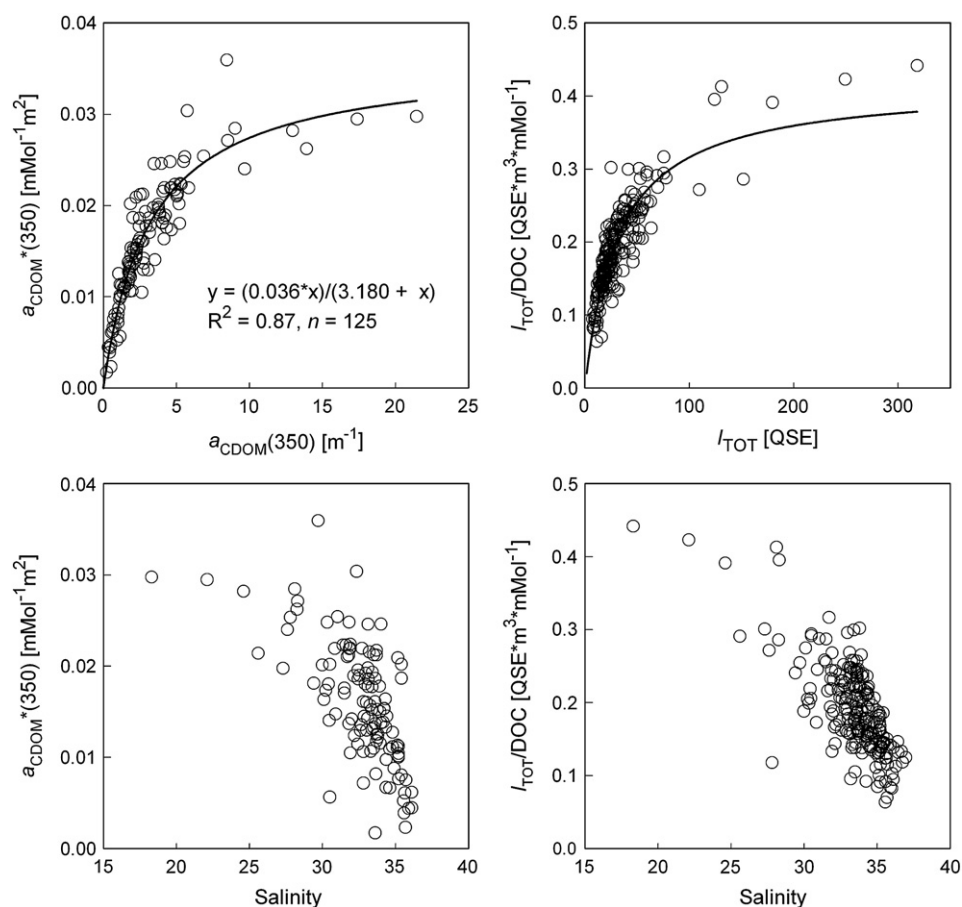


Fig. 6. Relationship between CDOM carbon-specific absorption coefficient ($a^*_{\text{CDOM}}(350)$) and CDOM absorption coefficient ($a_{\text{CDOM}}(350)$)—upper left panel. Relationship between CDOM carbon-specific total fluorescence intensity and the CDOM total fluorescence intensity (I_{TOT})—upper right panel. Relationship between CDOM carbon-specific absorption coefficient ($a^*_{\text{CDOM}}(350)$) and salinity—lower left panel. Relationship between CDOM carbon-specific total fluorescence intensity and salinity—lower right panel.

The spectral fluorescence of EEMs and the new method of analysis using a PARAFAC model provided information that could be utilized to resolve variability of the organic carbon-specific absorption CDOM coefficient in relation to CDOM composition. In five subplots of $a^*_{\text{CDOM}}(350)$ vs. different ratios of fluorescence intensities (Fig. 7), the intensity of the primary terrestrial humic-like C1 was used to normalize the intensities of other fluorescence components that were identified by the PARAFAC model. The decrease in values of the ratio $I_{\text{C}_n}/I_{\text{C}_1}$ reflected the increased significance of the primary humic-like component relative to the intensity of the specific CDOM component. Intensity of the humic-like component was inversely correlated with salinity (Kowalczyk et al., 2009). Therefore, the low value of the $I_{\text{C}_n}/I_{\text{C}_1}$ ratio was associated with the low-salinity end member of the present data set. There was an overall trend of a decrease of $a^*_{\text{CDOM}}(350)$ with an increase of the $I_{\text{C}_n}/I_{\text{C}_1}$ ratio. A purely statistical analysis was applied to quantify the effect of the CDOM compositional changes on the value of carbon-specific CDOM absorption coefficient, $a^*_{\text{CDOM}}(350)$. The type of fit was chosen based upon nearest proximity of the empirical distribution to the known properties of the analytical functions. The fits were optimized to achieve highest statistically significant values of the determination coefficient and regression coefficients at the given confidence level ($p < 0.01$). However, only two of the five generated $a^*_{\text{CDOM}}(350)$ distributions vs. $I_{\text{C}_n}/I_{\text{C}_1}$ ratios may be used for a reliable statistical model to predict CDOM organic carbon-specific absorption coefficients in the context of the qualitative composition of DOM.

Variability of $a^*_{\text{CDOM}}(350)$ may be best quantitatively resolved by changes in C2 and C5 intensities relative to changes in intensity of C1. Changes of $a^*_{\text{CDOM}}(350)$ values as a function of $I_{\text{C}_2}/I_{\text{C}_1}$ may be approximated by a linear regression, however the determination

coefficient (R^2) calculated for this relationship was smaller than the R^2 value calculated for other relationships between the carbon-specific CDOM absorption coefficient and ratio of fluorescence intensities of specific components (Table 3). The distribution of $a^*_{\text{CDOM}}(350)$ was well correlated with relative changes of intensity of the marine humic-like C3, normalized to the intensity of the primary terrestrial humic-like C1. Furthermore, the linear regression between those two parameters was significant with a high determination coefficient value ($R^2 = 0.60$). The use of this relationship for prediction of $a^*_{\text{CDOM}}(350)$ was limited due to a narrow range of variability in the $I_{\text{C}_3}/I_{\text{C}_1}$ ratio. The ratio of the secondary terrestrial humic-like component, C4, to the intensity of the primary terrestrial humic-like component, C1, does not contribute significantly to the variability of the organic carbon-specific absorption coefficient by CDOM. There was a clear non-linear distribution of the $a^*_{\text{CDOM}}(350)$ vs. $I_{\text{C}_5}/I_{\text{C}_1}$ ratio. One functional model, a power function, was used to predict variability of the CDOM organic carbon-specific absorption coefficients. Regression coefficients calculated for this model were statistically significant, and calculated R^2 was high (Table 3).

The last panel of Fig. 7 shows the changes of $a^*_{\text{CDOM}}(350)$ as a function of the $I_{\text{C}_4}/I_{\text{C}_5}$ ratio. This ratio was chosen to evaluate the sensitivity of the CDOM organic carbon-specific absorption coefficient value to the relative contribution of components associated with other fractions of DOM that have excitation and emission maxima situated at the longest wavelengths and represent organic substances with the largest molecular weight and highest aromaticity (secondary humic-like components C4). The intensity of C4 was normalized to the intensity of the protein-like C5, which is associated with autochthonous production of DOM. High values of the $I_{\text{C}_4}/I_{\text{C}_5}$ ratio represented a higher contribution of C4 compared to C5 within

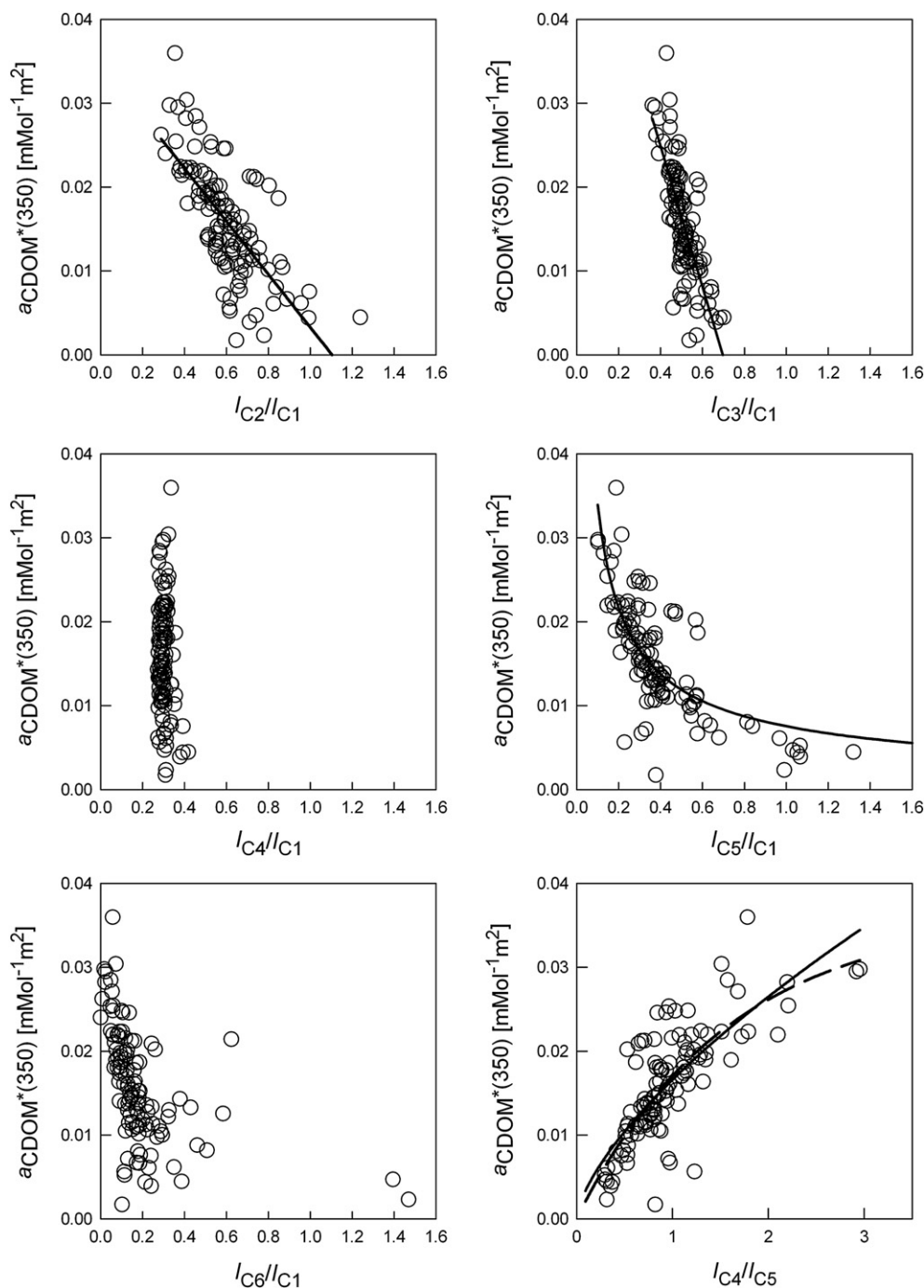


Fig. 7. Relationships between CDOM carbon-specific absorption coefficient ($a^*_{\text{CDOM}(350)}$) and ratio of respective fluorescence components identified by the PARAFAC model normalized to fluorescence intensity of the component C1. Upper right panel—solid line represents linear approximation of the relationship between $a^*_{\text{CDOM}(350)}$ and I_{C2}/I_{C1} . Upper right panel—solid line represents linear approximation of the relationship between $a^*_{\text{CDOM}(350)}$ and I_{C3}/I_{C1} ratio. Middle right panel—solid line represents power approximation of the relationship between $a^*_{\text{CDOM}(350)}$ and I_{C5}/I_{C1} ratio. Lower right panel—relationships between CDOM carbon-specific absorption coefficient ($a^*_{\text{CDOM}(350)}$) and the fluorescence intensity ratio of components C4 and C5. Solid line represents exponential approximation of the relationship between $a^*_{\text{CDOM}(350)}$ and I_{C4}/I_{C5} ratio, a dashed line represents a power approximation of the relationship between same parameters.

the total fluorescence intensity and were indicative of low-salinity estuarine or even fresh water samples. In contrast, low I_{C4}/I_{C5} ratios were indicative of oceanic water. Furthermore, the contribution of the C5 to the total fluorescence intensity may be several times higher compared to C4. There was a clear non-linear trend between the increase of $a^*_{\text{CDOM}(350)}$ with increase of the I_{C4}/I_{C5} ratio. Changes of these two parameters have been approximated using exponential and power functions. The exponential growth function better predicted changes of the CDOM organic carbon-specific absorption coefficient.

3.4. Estimation of the organic carbon discharge by the Cape Fear River to the coastal ocean

The results of a regression analysis between the values of $a_{\text{CDOM}(350)}$ measured at CFP1 during the whole period of the CORMP program (the sampling station closest to the river mouth) and the mean daily CFR flow measured at lock Kelly, N.C. (the flow data obtained from USGS survey) are presented in Fig. 8. There was a significant positive trend of increasing CDOM absorption coefficient with increasing river discharge. A non-linear regression was used to

Table 3
Results of regression analysis between $a_{\text{CDOM}}^*(350)$ and intensity ratios of individual components derived from the PARAFAC model.

Parameters	Equation type	Regression coefficients	Coefficient of determination R^2	Sample size n
$a_{\text{CDOM}}^*(350)$ vs. $a_{\text{CDOM}}(350)$	Hyperbola $y = a*x/(b+x)$	$a = 0.0361 \pm 0.0014$ $b = 3.1801 \pm 0.2615$	0.87	119
$a_{\text{CDOM}}^*(350)$ vs. I_{TOT}	Hyperbola $y = a*x/(b+x)$	$a = 0.4163 \pm 0.0125$ $b = 31.703 \pm 1.9517$	0.80	229
$a_{\text{CDOM}}^*(350)$ vs. $I_{\text{C2}}/I_{\text{C1}}$	Linear $y = a*x + b$	$a = -0.0316 \pm 0.0027$ $b = 0.0349 \pm 0.0017$	0.55	115
$a_{\text{CDOM}}^*(350)$ vs. $I_{\text{C3}}/I_{\text{C1}}$	Linear $y = a*x + b$	$a = -0.0838 \pm 0.0063$ $b = 0.0584 \pm 0.0032$	0.60	115
$a_{\text{CDOM}}^*(350)$ vs. $I_{\text{C5}}/I_{\text{C1}}$	Power $y = a*x^b$	$a = 0.0075 \pm 0.0006$ $b = -0.6562 \pm 0.0532$	0.59	115
$a_{\text{CDOM}}^*(350)$ vs. $I_{\text{C4}}/I_{\text{C5}}$	Exponential $y = a*(1 - \exp(-b*x))$	$a = 0.0365 \pm 0.0047$ $b = 0.6308 \pm 0.1202$	0.62	115
$a_{\text{CDOM}}^*(350)$ vs. $I_{\text{C4}}/I_{\text{C5}}$	Power $y = a*x^b$	$a = 0.0166 \pm 0.0004$ $b = 0.6745 \pm 0.0534$	0.59	115

All variables were fitted to equation type given in second column. All regression coefficients and coefficients of determination are significant at a confidence level $p < 0.01$.

fit the data and the power function gave the best fit results in terms of the coefficient of determination and statistical significance. This power function formula was used to reconstruct the daily average values of $a_{\text{CDOM}}(350)$. Estimates of the CDOM absorption coefficient were used in the inversion of the relationship between $a_{\text{CDOM}}(350)$ and DOC to calculate daily averaged concentration of DOC. The daily averaged loads of DOC were calculated based on estimated DOC concentrations and discharge volumes, which are dependent on flow. Those estimates of daily averaged loads of DOC were integrated for 2002, 2003 and 2004 to estimate the annual flux of DOC from the CFR to Long Bay in $\text{DOC g } 10^{10} \text{ yr}^{-1}$. The estimated annual DOC flux in these three years was variable. The flux of DOC in 2002, the year of the extreme drought in CFR watershed, was $1.5 \text{ g } 10^{10} \text{ yr}^{-1}$. This was 1/4th the DOC flux estimated in 2003, ($6.2 \text{ g } 10^{10} \text{ yr}^{-1}$), a period of extreme precipitation. The DOC flux in 2004, which was regarded as a “typical” year for hydrological regime in the coastal plain of the North Carolina, was $2.2 \text{ g } 10^{10} \text{ DOC yr}^{-1}$.

4. Discussion

The distribution of CDOM optical properties in the estuarine waters of the CFR plume area is controlled by precipitation in the watershed and flux of terrestrial organic matter through river discharge and its mixing with adjacent oceanic waters (Kowalczyk et al., 2003, 2009). Avery et al. (2003, 2004) presented evidence that the CFR is the most important source of organic matter in the CFR estuary. However, during extreme storm events direct rain deposition of organic carbon may reach 10% of the average annual discharge of

DOM. Although diffuse sources of organic matter are significant in the study area, Avery et al. (2004) reported conservative behavior of DOC along the salinity gradient from terrestrial source toward the open ocean. Therefore, we would expect strong covariance between CDOM optical properties and DOC distribution in the CFR plume area.

DOM fluorescence in natural waters has been used as a proxy for the CDOM absorption coefficient since the early 1960s (Duursma, 1965) and numerous investigators have observed a linear relationship between fluorescence and absorption coefficients (Ferrari and Tassan, 1991; Hoge et al., 1993; Vodacek et al., 1997; Ferrari and Dowell, 1998; Ferrari, 2000; Chen et al., 2002; Del Vecchio and Blough, 2004). Typically, the CDOM absorption coefficient at excitation wavelengths (usually around 350 nm) is correlated with the integrated fluorescence signal normalized to water Raman scattering peak (and sometimes standardized to quinine sulfate equivalents (QSE in ppb)). Published empirical relationships between the absorption coefficient and fluorescence have been derived from results of field data collected in various coastal, marine and estuarine environments in Europe, American Atlantic and the Pacific coasts (published coefficients of determination are usually higher than 0.9). The relationship in this study between $a_{\text{CDOM}}(350)$ and I_{TOT} may be regarded as linear since a broad range of variability and values of determination coefficients were slightly less than 0.9. It should be noted that I_{TOT} was calculated as the sum of components' intensities with different excitations; therefore, smaller values of R^2 were expected. The relationship between fluorescence and the CDOM absorption coefficient may be improved if the fluorescence intensity was expressed as the integral of the whole EEM. This approach was presented by Kowalczyk et al. (2003, 2005) and calculated R^2 values for those relationships were much higher (0.96) with the exception of protein-like fluorophores.

One possible reason for strong CDOM absorption vs. fluorescence relationships is the relative stability of the apparent quantum yield for CDOM fluorescence. Green and Blough (1994) published a record of CDOM fluorescence apparent quantum yields of surface waters from various sites along the Atlantic coast and documented an almost two orders of magnitude variation in $a_{\text{CDOM}}(355)$, while variation in the calculated CDOM fluorescence apparent quantum yield was only around 1%. The highest quantum yields were observed in ocean deep water (2.1%) and the lowest in freshwater environments (~0.4%). The regression was better for those components that had either excitation bands around 350 nm (secondary excitation maximum of C4) or a tail of excitation spectrum in this region (C1 and/or C3). The components that have excitation spectra in the UV-C region were least correlated with the $a_{\text{CDOM}}(350)$. The spectral characteristics of the EEM components identified by the PARAFAC model may explain some of the relative stability of fluorescence quantum yields in oceanic coastal waters. Light at 350 nm excites mainly humic-like fluorophores and secondary humic-like fluorophores emit in the visible spectrum.

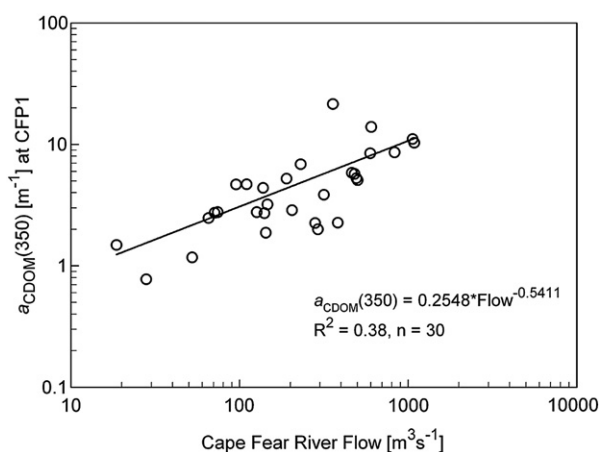


Fig. 8. A relationship between CDOM absorption coefficient ($a_{\text{CDOM}}(350)$) at the sampling station CFP1 and Cape Fear River flow.

Those components are abundant in coastal and estuarine waters and dominate the DOM composition (Stedmon et al., 2003; Stedmon and Markager, 2005a). Therefore, light emitted by excited fluorophores may be re-absorbed by fluorophores that have excitation spectra extended into visible light, hence reducing the overall fluorescence efficiency.

The marine humic-like component, C3, has a secondary excitation band around 350 nm and is most susceptible to bacterial reworking (Stedmon and Markager, 2005b). In open ocean waters, humic-like components are usually less abundant and protein-like and marine humic-like components dominate (Murphy et al., 2008; Kowalczyk et al., 2009). The appearance of C3 is attributed to bacterial reworking of DOM and contributes to fluorophores with excitation and emission characteristics situated at short wavelengths. This leads to an increase of the quantum yield of CDOM in deep oceanic waters relative to coastal, estuarine and freshwater environments.

The relationship between CDOM optical properties and the concentration of DOC has been studied in various waters for the last three decades and was based on an assumption of conservative behavior of these parameters at local scales, which justified empirical regressions of $a_{\text{CDOM}}(\lambda)$ vs. DOC. This assumption is valid in many coastal areas dominated by riverine outflow and there are numerous reports presenting empirical relationships between CDOM optical properties and DOC concentrations (e.g., Nyquist, 1979; Vodacek et al., 1995; Ferrari et al., 1996). However, later it was shown that optical properties of CDOM are not conservative and change due to CDOM degradation processes such as photochemical reactions and bacterial grazing, which also lead to seasonal variability in $a_{\text{CDOM}}(\lambda)$ vs. DOC relationships in the coastal ocean (Vodacek et al., 1997; Rochelle-Newall and Fisher, 2002; Del Vecchio and Blough, 2004; Mannino et al., 2008). The data in this study do not show any seasonal variation in a linear relationship between $a_{\text{CDOM}}(350)$, I_{TOT} and DOC concentrations. The absence of a seasonal dependency in the presented relationships may be explained by the dominant role of terrestrial sources in the export of organic matter to the CFR estuary. CDOM optical properties resulting from physical, biochemical and microbial alteration of terrestrial organic material are suppressed by the very high terrestrial CDOM signal. This seems to occur along the entire salinity gradient from the terrestrial into the oceanic end member. However, alteration of DOM may be observed in natural environments under favorable conditions, where freshwater input of DOM has been diluted sufficiently enough and DOM is trapped within the shallow mixing zone under exposure to solar radiation (Helms et al., 2008). This is not the case for the well-mixed tidal CFR estuary, which has an average water residence time of 7 days. In the CFR plume area, conservative mixing controls the distribution of CDOM optical properties up to near-oceanic salinities of about 34 (Kowalczyk et al., 2003).

To our knowledge, a relationship between intensity of fluorescence components derived from PARAFAC model vs. DOC has not been published previously and this study attempted to show these relationships. The results of this study need to be confirmed by future studies, with a specific focus on the relationship between the intensity of protein-like fluorophores with DOC concentrations, where the intercept was negligible. Non-absorbing DOC fractions with values around 80–10 $\mu\text{mol/l}$ have been reported by other researchers (Rochelle-Newall and Fisher, 2002; Mannino et al., 2008) in coastal ocean and estuarine areas and they indicate the size of the optically inactive pool of organic matter and limits of DOC detection using optical measurements in the visible and UV-A spectral range. This fraction was smaller (smaller x-intercept value) for components representing organic compounds with smaller molecular weight. The range in variability in the intercepts in our data is comparable to published data from other locations on the U.S. Atlantic coast (Vodacek et al., 1997; Del Vecchio and Blough, 2004; Mannino et al., 2008).

The lowest value of the CDOM-specific absorption coefficient, $a^*_{\text{CDOM}}(350) = 0.00172 \text{ m}^2 \text{ mmol}^{-1}$, reported in our study is in the same range

as reported by Del Vecchio and Blough (2004) for samples from the shelf break waters in the Middle Atlantic Bight. The highest value of this coefficient, $a^*_{\text{CDOM}}(350) = 0.03596 \text{ m}^2 \text{ mmol}^{-1}$, observed in the CFR estuary significantly exceeds values observed in Chesapeake Bay and Delaware Bay. The CDOM-specific absorption coefficients in this study were compared with those published by Carder et al. (1989) for fulvic and humic acids isolated from waters of the Gulf of Mexico after appropriate conversion of DOC concentration units (from $\mu\text{mol/l}$ into g/m^3) and spectral adjustment of the CDOM absorption coefficient. The lowest value of $a^*_{\text{CDOM}}(450)$, (in $\text{m}^2 \text{ g}^{-1}$) in our data set is an order of magnitude higher than a $a^*_{\text{CDOM}}(450)$ value for isolated fulvic acids published by Carder et al. (1989). The highest values of $a^*_{\text{CDOM}}(450)$ in our data set, although the same order of magnitude, are three times higher than the same parameter observed for isolated humic acids in the Gulf of Mexico. Our values are almost the same as the values for specific absorption coefficients estimated for humic acids extracted from soils (Zepp and Schlotzhauer, 1981). The discrepancy between our data and values reported by Carder et al. (1989), especially in waters least influenced by the CFR plume, can be explained by the CDOM EEM components derived from the PARAFAC model. Kowalczyk et al. (2009) showed that terrestrial humic-like material significantly contributes to the total CDOM fluorescence intensity, even in the coastal ocean outside the direct impact of the CFR plume. Very high values of the CDOM-specific absorption coefficient observed in the CFR estuary suggest that terrestrial DOM exported from the coastal plain by a river is highly concentrated.

The value of $a^*_{\text{CDOM}}(350)$ decreased quickly with increasing salinity, as shown in Fig. 5. This trend matches very well the spatial distribution of $a^*_{\text{CDOM}}(355)$ in the Middle Atlantic Bight reported by Del Vecchio and Blough (2004). This trend can be modeled using a hyperbolic function when salinity was substituted with $a_{\text{CDOM}}(350)$ and I_{TOT} values. High values of $a_{\text{CDOM}}(350)$ and I_{TOT} represent terrigenous DOM, which has much higher molecular weight than marine DOM (Harvey et al., 1983; Carder et al., 1989). Derived statistical hyperbolic relationships between $a^*_{\text{CDOM}}(350)$ and $a_{\text{CDOM}}(350)$, and between $I_{\text{TOT}}/\text{DOC}$ and I_{TOT} may be very useful for predicting values of the carbon-specific CDOM absorption coefficient and carbon-specific fluorescence intensity. A similar model was suggested by Stiiig Markager at the ASLO Summer meeting in Charleston, S.C, USA in 2004 for the global distribution of $a_{\text{CDOM}}(\lambda)$ and $a^*_{\text{CDOM}}(\lambda)$ values (personal communication). However, these models have not been published in the peer reviewed literature. Decreases of CDOM fluorescence intensity/DOC concentration ratios across broad salinity ranges, from fresh to oceanic waters, have been reported by Callahan et al. (2004). However, their distribution was close to linear, and did not have sharp inflection points as the one presented in Fig. 5.

The asymptotic increase of $a^*_{\text{CDOM}}(350)$ toward the terrestrial source needs to be confirmed by other studies. Jaffé et al. (2008) recently presented a trend of increased CDOM-specific absorption coefficient in the UV range (the SUVA index) as a function of DOC concentration. DOC concentration is usually well correlated with CDOM absorption in various aquatic environments and the distribution of SUVA presented in that study supports our model. However, Jaffé et al. (2008) did not present any functional approximation of trends from their data set. The distribution of the CDOM carbon-specific absorption coefficient as a function of the mass proxy ($a_{\text{CDOM}}(350)$) is distinctly different from the observed distribution of the mass-specific absorption coefficient of phytoplankton pigments as a function of chlorophyll *a* concentration (Woźniak and Dera, 2007). Therefore, further studies of exact physical and chemical mechanisms that lead to such distributions of CDOM-specific absorption coefficients with parameters related to mass should be presented.

Observations using EEM fluorescence spectroscopy provide evidence that CDOM composition changes substantially during transition from terrestrial sources to the open ocean (Stedmon et al., 2003; Kowalczyk et al., 2003; Stedmon and Markager, 2005a; Murphy et al., 2008; Yamashita et al., 2008). These changes impact variability in

the CDOM-specific absorption coefficient, $a^*_{\text{CDOM}}(350)$, which was demonstrated by the correlation of this coefficient with the fluorescence intensity ratios of specific components. Results presented in our study suggest that variability of $a^*_{\text{CDOM}}(350)$ is primarily controlled by mutual ratios of terrestrial humic-like components vs. protein-like components. A statistical model was developed that may be used to predict a CDOM carbon-specific absorption coefficient. However, this may only be applicable for local conditions in the South Atlantic Bight. The trend of a decrease in the CDOM carbon-specific absorption coefficient with decreased contribution of humic-like material to the fluorescence intensity was previously presented by Jaffé et al. (2008). They reported a statistically significant inverse linear relationship between the fluorescence index (FI) versus SUVA for a data set collected in a variety of freshwater and coastal sites around the USA. The increase of FI was associated with a decrease in the terrestrial humic-like fraction of DOM. Hence, a decrease of terrestrial humic-like fluorescence intensity is associated with a decrease of CDOM-specific absorption, which closely matches the trend in our data.

Another indirect qualitative confirmation of the model in this study was reported in the study by Ylöstalo et al. (2009) from the Baltic Sea. They presented a very good statistical relationship between the CDOM absorption spectrum slope coefficient (S) vs. CDOM carbon-specific absorption coefficient $a^*_{\text{CDOM}}(375)$. Specific absorption decreased with increased spectral slope. High spectral slope values are usually associated with CDOM that has been modified by photobleaching (e.g., Grzybowski, 2000), but may also be result of the mixing of different water masses with distinctly different CDOM optical properties (Stedmon and Markager, 2003; Kowalczuk et al., 2006b). Therefore, the impact of CDOM compositional changes due to different degradation processes on the specific absorption coefficient deserves further study.

Significant correlations among the CDOM absorption coefficient, the total fluorescence intensity and DOC concentration can be used to predict the annual discharge of DOC. Empirical relationships between CDOM optical properties and DOC concentration have previously been used to estimate the input of organic carbon to the coastal ocean in the Orinoco River plume (e.g., Blough et al., 1993). Optical properties of CDOM may be estimated from ocean color satellite observations, which may be used to map DOC concentrations using satellite imagery. This approach has been tested recently by Del Castillo and Miller (2008) in the Mississippi plume area and by Mannino et al. (2008) in the Middle Atlantic Bight. In our study, optical data and relationships between CDOM optical characteristics and DOC concentration were used to estimate an annual load of organic carbon exported to the coastal ocean by the CFR. Previous estimates of DOC fluxes in the CFR were based on an average DOC concentration in the North CFR and Black River and an average CFR flow (Avery et al., 2003, 2004). Those calculations were based on the mean DOC concentration in CFR tributaries above the city of Wilmington and CFR flow data from USGS. CFR flow is highly variable and responds very quickly to changes in the hydrological regime which impacts the quality and quantity of DOM within this river (Kowalczuk et al., 2009). The mean annual discharge is usually less than the standard deviation (Carpenter and Yonts, 1979). Therefore, estimates of DOC flux based on the mean annual discharge are severely overestimated during drought periods and may be underestimated during high-flow events. Our estimation of the annual DOC export of the CFR to the coastal ocean during high-flow conditions agrees with estimations published by Avery et al. (2003). However, our approach can provide additional and more detailed information on temporal variability of the DOC flux. The input of the terrestrial CDOM and its composition are controlled by CFR flow (Kowalczuk et al., 2009). Therefore, relationships between river flow and the CDOM absorption coefficient enabled us to estimate the DOM optical properties on a daily time scale. Integration of the daily DOC flux estimated from the relationship between a_{CDOM}

(350) and DOC on different time scales allows observations on the temporal variability of DOC export to the coastal ocean. In this study, it was demonstrated that during a drought in the CFR watershed the annual export of DOC decreased by a factor of four. Temporal variability of DOC export has significant ecological implications. DOM carries substantial concentrations of dissolved organic nitrogen (DON) and dissolved organic phosphorus (DOP), which are gradually remineralized into inorganic forms through photochemical and microbial DOM degradation processes (e.g., Vähätalo and Zepp, 2005; Stedmon et al., 2007). Thus, the pulse of riverine DOM export may act as additional source of nutrients and support growth of phytoplankton communities in areas outside the direct impact of fresh water plume.

5. Conclusions

The results of this study demonstrate that it is possible to obtain an accurate estimation of DOC export by the Cape Fear River using optical measurements. Optical measurements are convenient, fast, relatively inexpensive, and provide DOC flux estimates with increased temporal resolution. Both fluorometers and absorption or attenuation meters, like the AC-9 instrument, may be installed on autonomous platforms as moorings or gliders and extend the spatial coverage of DOC monitoring. This study suggests that it is possible to estimate the CDOM carbon-specific absorption coefficient through CDOM absorption measurements and that the value of $a^*_{\text{CDOM}}(350)$ is controlled by changes in CDOM composition. Application of PARAFAC models enables the identification of DOM components that control $a^*_{\text{CDOM}}(350)$ value distributions in the transition zone between estuary and coastal ocean. The $a^*_{\text{CDOM}}(350)$ values are controlled to a great extent by the ratios of terrestrial humic-like components and protein-like components. Careful spectral adjustments of excitation wavebands may enable measurements of different DOM fractions, and possibly significantly reduce the estimates of the non-absorbing DOC fraction in optical methods for DOC measurements and improve the accuracy of DOC estimation.

Acknowledgements

This study was supported 1 by NOAA (Grant No. NA16RP2675) through the Coastal Ocean Research and Monitoring Program, Center for Marine Science, University 3 of North Carolina at Wilmington, and by Statutory Research Program no. II.5, at the Institute of Oceanology, Polish Academy of Sciences, Sopot, Poland. Partial financial support was provided by the research grant no. NN306 2942 33 awarded to PK by the Polish Ministry of Science and Higher Education. The development of the Fluorescence Toolbox was supported by Office of Naval Research grant N00014-98-1-0530 awarded to Richard G. Zepp (U.S.E.P.A.) and Mary Ann Moran (University of Georgia). Authors would like to acknowledge Wade Sheldon, University of Georgia, Athens, USA, for his kind permission to use the Fluorescence Toolbox software. Also, we would like to thank Colin A. Stedmon and Stiig Markager from National Environmental Research Institute, Roskilde, Denmark, for consultations and Matlab scripts for PARAFAC modeling. Authors would like to acknowledge comments provided by the associate editor and the reviewers, which improved the quality of the manuscript. This is contribution 40 from the University of California, Irvine, Urban Water Research Center.

References

- Andersson, C.A., Bro, R., 2000. The N-way toolbox for MATLAB. *Chemometrics Intelligent Laboratory System* 52, 1–4.
- Oceanography of southeastern U.S. continental shelf. In: Atkinson, L.P., Menzel, D.W., Bush, K.A. (Eds.), *Coastal Estuarine Sci. Ser.*, vol. 2. AGU, Washington D.C. 156 pp.
- Avery Jr., G.B., Willey, J.D., Kieber, R.J., Shank, G.C., Whitehead, R.F., 2003. Flux and bioavailability of Cape Fear River and rainwater dissolved organic carbon to Long Bay, southeastern United States. *Global Biogeochemical Cycles* 17 (2), 1042. doi:10.1029/2002GB001964.

- Avery Jr., G.B., Kieber, R.J., Willey, J.D., Shank, G.C., Whitehead, R.F., 2004. Impact of hurricanes on the flux of rainwater and Cape Fear River water dissolved organic carbon to Long Bay, southeastern United States. *Global Biogeochemical Cycles* 18, GB3015. doi:10.1029/2004GB002229.
- Blough, N.V., Zafriou, O.C., Bonilla, J., 1993. Optical absorption spectra of waters from the Orinoco River outflow: terrestrial input of coloured organic matter to the Caribbean. *Journal of Geophysical Research* 98, 2271–2278.
- Blough, N.V., Del Vecchio, R., 2002. Chromophoric DOM in the coastal environment. In: Hansell, D., Carlson, C. (Eds.), *Biogeochemistry of Marine Dissolved Organic Matter*. Academic Press, New York, pp. 509–546.
- Bro, R., 1997. PARAFAC. Tutorial and applications. *Chemometrics Intelligent Laboratory System* 38, 149–171.
- Carder, K.L., Steward, R.G., Harvey, G.R., Ortner, P.B., 1989. Marine humic and fulvic acids. Their effect on remote sensing of ocean chlorophyll. *Limnology and Oceanography* 34, 68–81.
- Carpenter, J.L., Yonts, W.L., 1979. Dytracer and current meter studies Cape Fear Estuary, N. C. Report to Carolina Power and Light Company. 74 pp.
- Callahan, J., Dai, M., Chen, R.F., Li, X., Lu, Z., Huang, W., 2004. Distribution of dissolved organic matter in the Pearl River Estuary, China. *Marine Chemistry* 89, 211–224.
- Chen, R.F., Zhang, Y., Vlahos, P., Rudnick, S.M., 2002. The fluorescence of dissolved organic matter in the Mid-Atlantic Bight. *Deep-Sea Research II* 49, 4439–4459.
- Coble, P.G., 2007. Marine optical biogeochemistry: the chemistry of ocean color. *Chemical Reviews* 107 (2), 402–418.
- Coble, P.G., Schultz, C.A., Mopper, K., 1993. Fluorescence contouring analysis of DOC Inter-calibration Experiment samples: a comparison of techniques. *Marine Chemistry* 41, 175–178.
- Coble, P.G., Del Castillo, C.E., Avril, B., 1998. Distribution and optical properties of CDOM in the Arabian Sea during the 1995 Southwest Monsoon. *Deep-Sea Research II* 45, 2195–2223.
- Del Castillo, C.E., 2005. Remote sensing of organic matter in coastal waters. In: Miller, R.L., Del Castillo, C.E., McKee, B.A. (Eds.), *Remote Sensing of Coastal Aquatic Environments*. Springer, Dordrecht, Netherlands, 347 pp.
- Del Castillo, C.E., Miller, R.L., 2008. On the use of ocean color remote sensing to measure the transport of dissolved organic carbon by the Mississippi River Plume. *Remote Sensing of Environment* 112, 836–844.
- Del Vecchio, R., Blough, N.V., 2004. Spatial and seasonal distribution of chromophoric dissolved organic matter and dissolved organic carbon in the Middle Atlantic Bight. *Marine Chemistry* 89, 169–187.
- Duursma, E.K., 1965. The dissolved organic constituents of seawater. In: Riley, J.P., Skirrow, G. (Eds.), *Chemical Oceanography*, vol. 1. Academic Press, London, pp. 433–475.
- Ferrari, G.M., 2000. The relationship between chromophoric dissolved organic matter and dissolved organic carbon in the European Atlantic coastal area and in the West Mediterranean Sea (Gulf of Lions). *Marine Chemistry* 70, 339–357.
- Ferrari, G., Tassan, S., 1991. On the accuracy of determining light absorption by "yellow substance" through measurements of induced fluorescence. *Limnology and Oceanography* 36 (4), 777–786.
- Ferrari, G.M., Dowell, M.D., Grossi, S., Targa, C., 1996. Relationship between optical properties of chromophoric dissolved organic matter and total concentration of dissolved organic carbon in southern Baltic Sea region. *Marine Chemistry* 55, 299–316.
- Ferrari, G.M., Dowell, M.D., 1998. CDOM absorption characteristics with relation to fluorescence and salinity in coastal areas of the southern Baltic Sea. *Estuarine, Coastal and Shelf Science* 47, 91–105.
- Gonsior, M.B.M., Peake, W.T., Cooper, D., Podgorski, D., Andriulli, J., Cooper, W.J., 2009. Photochemically induced changes in dissolved organic matter identified by ultrahigh resolution Fourier transform-ion cyclotron resonance mass spectrometry. *Environmental Science and Technology* 43, 698–703.
- Green, S.A., Blough, N.V., 1994. Optical absorption and fluorescence properties of chromophoric dissolved organic matter in natural waters. *Limnology and Oceanography* 39, 1903–1916.
- Grzybowski, W., 2000. Effect of short-term sunlight irradiation on absorbance spectra of chromophoric organic matter dissolved in coastal and riverine water. *Chemosphere* 40, 1313–1318.
- Hansell, D.A., Carlson, C.A., 1998. Deep-ocean gradients in the concentration of dissolved organic carbon. *Nature* 395 (6699), 263–266.
- Hansell, D.A., Carlson, C.A., 2001. Marine dissolved organic matter and the carbon cycle. *Oceanography* 14 (4), 41–49.
- Hansell, D., Carlson, C. (Eds.), 2002. *Biogeochemistry of Marine Dissolved Organic Matter*. Academic Press, New York, pp. 509–546.
- Hargreaves, B.R., 2003. Water column optics and penetration of UVR. In: Helbling, E.W., Zagarese, H. (Eds.), *UV Effects in Aquatic Organisms and Ecosystems*, Vol. 1. The Royal Society of Chemistry, Cambridge UK, pp. 59–108.
- Harvey, G.R., Boran, D.A., Chesal, L.A., Tokar, J.M., 1983. The structure of marine fulvic and humic acids. *Marine Chemistry* 12, 119–132.
- Hedges, J.L., 2002. Why dissolved organic matter. In: Hansell, D., Carlson, C. (Eds.), *Biogeochemistry of Marine Dissolved Organic Matter*. Academic Press, New York, pp. 1–33.
- Helms, J.R., Stubbins, A., Ritchie, J.D., Minor, E.C., Kieber, D.J., Mopper, K., 2008. Absorption spectral slopes and slope ratios as indicators of molecular weight, source, and photobleaching of chromophoric dissolved organic matter. *Limnology and Oceanography* 53, 955–969.
- Hoge, F.E., Vodacek, A., Blough, N.V., 1993. Inherent optical properties of the ocean: retrieval of the absorption coefficient of chromophoric dissolved organic matter from fluorescence measurements. *Limnology and Oceanography* 38 (7), 1394–1402.
- IOCCG, 2000. Remote sensing of the ocean colour in the coastal and other optically-complex waters. In: Sathyendranath, S. (Ed.), *Reports of the International Ocean-Colour Coordinating Group*, No. 3. IOCCG, Dartmouth, Canada. 140 pp.
- Jaffé, R., McKnight, D., Maie, N., Cory, R., McDowell, W.H., Campbell, J.L., 2008. Spatial and temporal variations in DOM composition in ecosystems: the importance of long-term monitoring of optical properties. *Journal of Geophysical Research* 113, G04032. doi:10.1029/2008JG000683.
- Jerlov, N.G., 1976. *Marine Optics*. Elsevier, New York. 231 pp.
- Johannessen, S.C., Miller, W.L., Cullen, J.J., 2003. Calculation of UV attenuation and colored dissolved organic matter absorption spectra from measurements of ocean color. *Journal of Geophysical Research* 108 (C9), 3301. doi:10.1029/2000JC000514.
- Kalle, K., 1966. The problem of the Gelbstoff in the sea. *Oceanography and Marine Biology. Annual Review* 4, 91–104.
- Kirk, J.T.O., 1994. *Light and Photosynthesis in Aquatic Ecosystems*, 2nd ed. Cambridge University Press, New York. 509 pp.
- Kowalczuk, P., Cooper, W.J., Whitehead, R.F., Durako, M.J., Sheldon, W., 2003. Characterization of CDOM in organic rich river and surrounding coastal ocean in the South Atlantic Bight. *Aquatic Sciences* 65, 384–401.
- Kowalczuk, P., Stoř-Egiert, J., Cooper, W.J., Whitehead, R.F., Durako, M.J., 2005. Characterization of chromophoric dissolved organic matter (CDOM) in the Baltic Sea by excitation emission matrix fluorescence spectroscopy. *Marine Chemistry* 96, 273–292.
- Kowalczuk, P., Durako, M.J., Cooper, W.J., Wells, D., Souza, J.J., 2006a. Comparison of radiometric quantities measured in water, above water and derived from SeaWiFS imagery in the South Atlantic Bight, North Carolina, USA. *Continental Shelf Research* 26, 2433–2453.
- Kowalczuk, P., Stedmon, C.A., Markager, S., 2006b. Modeling absorption by CDOM in the Baltic Sea from season, salinity and chlorophyll. *Marine Chemistry* 101, 1–11.
- Kowalczuk, P., Cooper, W.J., Durako, M.J., Young, H., Kahn, A.E., 2009. Characterization of dissolved organic matter fluorescence in the South Atlantic Bight with use of PARAFAC model: interannual variability. *Marine Chemistry* 113, 182–196.
- Mallin, M.A., Burkholder, J.M., Cahoon, L.B., Posey, M.H., 2000. North and South Carolina coast. *Marine Pollution Bulletin* 41, 56–75.
- Mannino, A., Russ, M.E., Hooker, S.B., 2008. Algorithm development and validation for satellite-derived distributions of DOC and CDOM in the U.S. Middle Atlantic Bight. *Journal of Geophysical Research* 113, C07051. doi:10.1029/2007JC004493.
- McKnight, D.M., Boyer, E.W., Westerhoff, P.K., Doran, P.T., Kulbe, T., Andersen, D.T., 2001. Spectrofluorometric characterization of dissolved organic matter for indication of precursor organic material and aromaticity. *Limnology and Oceanography* 46, 38–48.
- Mopper, K., Kieber, D.J., 2002. Photochemistry and the cycling of carbon, sulfur, nitrogen and phosphorus. In: Hansell, D.A., Carlson, C.A. (Eds.), *Biogeochemistry of Marine Dissolved Organic Matter*. Academic Press, New York, pp. 455–507.
- Mopper, K., Zhou, X., Kieber, R.J., Kieber, D.J., Sikorski, R.J., Jones, R.D., 1991. Photochemical degradation of dissolved organic carbon and its impact on the oceanic carbon cycle. *Nature* 353, 60–62.
- Moran, A.M., Sheldon, W.M., Zepp, R.G., 2000. Carbon loss and optical property changes during long-term photochemical and biological degradation of estuarine dissolved organic matter. *Limnology and Oceanography* 45, 1254–1264.
- Murphy, K.R., Stedmon, C.A., Waite, T.D., Ruiz, G.M., 2008. Distinguishing between terrestrial and autochthonous organic matter sources in marine environments using fluorescence spectroscopy. *Marine Chemistry* 108, 40–58.
- Nelson, N.B., Siegel, D.A., Michaels, A.F., 1998. Seasonal dynamics of colored dissolved material in the Sargasso Sea. *Deep Sea Research I* 45, 931–957.
- Nelson, N.B., Siegel, D.A., 2002. Chromophoric DOC in open ocean. In: Hansell, D., Carlson, C. (Eds.), *Biogeochemistry of Marine Dissolved Organic Matter*. Academic Press, New York, pp. 547–578.
- Nelson, N.B., Siegel, D.A., Carlson, C.A., Swana, C., Smethie Jr., W.M., Khattiwala, S., 2007. Hydrography of chromophoric dissolved organic matter in the North Atlantic. *Deep-Sea Research I* 54, 710–731.
- Nyquist, G., 1979. Investigation of some optical properties of sea water with special reference to lignin sulfonates and humic substances. Ph.D. thesis, Department of Analytical and Marine Chemistry, Göteborg University, Göteborg, Sweden, 203 pp.
- Opsahl, S., Benner, R., 1997. Distribution and cycling of terrigenous dissolved organic matter in the ocean. *Nature* 386, 480–482.
- Rochelle-Newall, E.J., Fisher, T.R., 2002. Chromophoric dissolved organic matter and dissolved organic carbon in Chesapeake Bay. *Marine Chemistry* 77, 23–41.
- Siegel, D.A., Maritorena, S., Nelson, N.B., Hansell, D.A., Lorenzi-Kayser, M., 2002. Global distribution and dynamics of colored dissolved and detrital organic materials. *Journal of Geophysical Research* 107 (C12), 3228. doi:10.1029/2001JC000965.
- Stedmon, C.A., Markager, S., 2003. Behaviour of the optical properties of coloured dissolved organic matter under conservative mixing. *Estuarine, Coastal and Shelf Science* 57, 973–979.
- Stedmon, C.A., Markager, S., 2005a. Resolving the variability in dissolved organic matter fluorescence in a temperate estuary and its catchment using PARAFAC analysis. *Limnology and Oceanography* 50, 686–697.
- Stedmon, C.A., Markager, S., 2005b. Tracing the production and degradation of autochthonous fractions of dissolved organic matter using fluorescence analysis. *Limnology and Oceanography* 50, 1415–1426.
- Stedmon, C.A., Markager, S., Kaas, H., 2000. Optical properties and signatures of chromophoric dissolved organic matter (CDOM) in Danish coastal waters. *Estuarine, Coastal and Shelf Science* 51, 267–278.
- Stedmon, C.A., Markager, S., Bro, R., 2003. Tracing dissolved organic matter in aquatic environments using a new approach to fluorescence spectroscopy. *Marine Chemistry* 82, 239–254.
- Stedmon, C.A., Markager, S., Tranvik, L., Kronberg, L., Slätis, T., Martinsen, W., 2007. Photochemical production of ammonium and transformation of dissolved organic matter in the Baltic Sea. *Marine Chemistry* 104, 227–240.

- Vähätalo, A.V., Zepp, R.G., 2005. Photochemical mineralisation of dissolved organic nitrogen to ammonium in the Baltic Sea. *Environmental Science and Technology* 39, 6985–6992.
- Vodacek, A., Hoge, F., Swift, R.N., Yungel, J.K., Peltzer, E.T., Blough, N.V., 1995. The use of in situ and airborne fluorescence measurements to determine UV absorption coefficients and DOC concentrations in surface waters. *Limnology and Oceanography* 40, 411–415.
- Vodacek, A., Blough, N.V., DeGrandpre, M.D., Peltzer, E.T., Nelson, R.K., 1997. Seasonal variation of CDOM and DOC in the Middle Atlantic Bight: terrestrial inputs and photooxidation. *Limnology and Oceanography* 42 (2), 674–686.
- Woźniak, B., Dera, J., 2007. *Light Absorption in Sea Water*. Springer, Dordrecht, Netherlands. 456 pp.
- Yamashita, Y., Jaffé, R., Maie, N., Tanoue, E., 2008. Assessing the dynamics of dissolved organic matter (DOM) in coastal environments by excitation emission matrix fluorescence and parallel factor analysis (EEM-PARAFAC). *Limnology and Oceanography* 53, 1900–1908.
- Ylöstalo P., J. Seppälä, and S. Kaitala, 2009. Spatial and seasonal variations in CDOM absorption and DOC/N concentrations in the Baltic Sea sub-basins. *Journal of Geophysical Research*, in revision.
- Zepp, R., Schlotzhauer, P.F., 1981. Comparison of photochemical behaviour of various humic substances in water: 3. Spectroscopic properties of humic substances. *Chemosphere* 10, 479–486.
- Zepp, R.G., Sheldon, W.M., Moran, M.A., 2004. Dissolved organic fluorophores in southeastern U.S. coastal waters: correction method for eliminating Rayleigh and Raman scattering peaks in excitation–emission matrices. *Marine Chemistry* 89, 15–36.